Supplementary Information (SI) for Nanoscale Horizons.

Understanding the Effects of Adduct Functionalization on C_{60} Nanocages for the Hydrogen Evolution Reaction

Joy Spears,[1] Mina Shawky Adly,[2] Edison Castro,[3] Alain R. Puente Santiago,[4*] Luis Echegoyen,[3] Tianwei He,[5*] Christopher J. Dares,[4] and Mohamed Noufal[1*]

[1]Department of Chemical Engineering, Hampton University, Hampton, VA 23668, USA.

[2]Deparment of Chemistry, Faculty of Science, Mansoura University, Al-Mansoura 35516, Egypt.

[3] Department of Chemistry, University of Texas at El Paso, 500 West University Avenue, El Paso, Texas 79968, United States

[4] Florida International University (FIU), Department of Chemistry and Biochemistry, Miami, FL, USA.

[5]National Center for International Research on Photoelectric and Energy Materials, Yunnan Key Laboratory for Micro/Nano Materials& Technology, School of Materials and Energy, Institute of International Rivers and Eco-Security, Yunnan University, Kunming 650091, China

KEYWORDS: Low-dimensional materials, 0D-Fullerenes, Functionalized fullerenes, Bis-pyrrolidine hexa-adducts of C_{60}, HER

Supporting information 1: Materials synthesis and characterization

C_{60}-tetra-malonate (C_{60}-TM) was synthesized as per a previously reported procedure. Penta-adduct and hexa-adduct were obtained by reacting C_{60}-TM with methyl glycine ester, using diacetoxyiodobenzene (DIB) and sodium carbonate decahydrate in ortho-dichlorobenzene (o-DCB) under sonication at ambient conditions **(Figure 1)**. Within half an hour, the solution changed to orange, indicating penta as the predominant product. Crystallization of the functionalized compounds was achieved through complexation with $ZnBr_2$ via slow evaporation in a benzene/chloroform/ethanol (9:9:1) solvent mixture. The coordination geometry of Zn1 is between trigonal bipyramidal and square pyramidal.[1] [2] Subsequently, H-C_{60} and P-C_{60} were synthesized via the reaction of C_{60}-TM (50 mg, 0.04 mmol) with methyl glycine ester hydrochloride (20 mg, 0.16 mmol), utilizing diacetoxyiodobenzene (39 mg, 0.12 mmol) and sodium carbonate decahydrate (37 mg, 0.13 mmol) in o-DCB (10 mL), under sonication and darkness at room temperature. The reaction mixture underwent a color change to orange after 30 minutes, whereas after 3 hours, it turned yellow, indicating the adduct as the main product, as observed by TLC using DCM/EA 30:1. Column chromatography purification facilitated the characterization of separated compounds using MALDI-TOF-MS and NMR spectroscopy. The synthesis of hexa-adduct involved reacting C_{60}-TM (50 mg, 0.04 mmol) with 2-pycolylamine (17 mg, 0.16 mmol) and 2-pyridinecarbaldehyde (17 mg, 0.16 mmol) in o-DCB (10 mL) under reflux conditions. A 30-minute reaction time yielded a yellow solution, with hex adduct being the sole product, confirmed by TLC using $CHCl_3$/MeOH 15:1. Subsequent column chromatography purification enabled characterization of hexa adduct via MALDI-TOF-MS and NMR spectroscopy

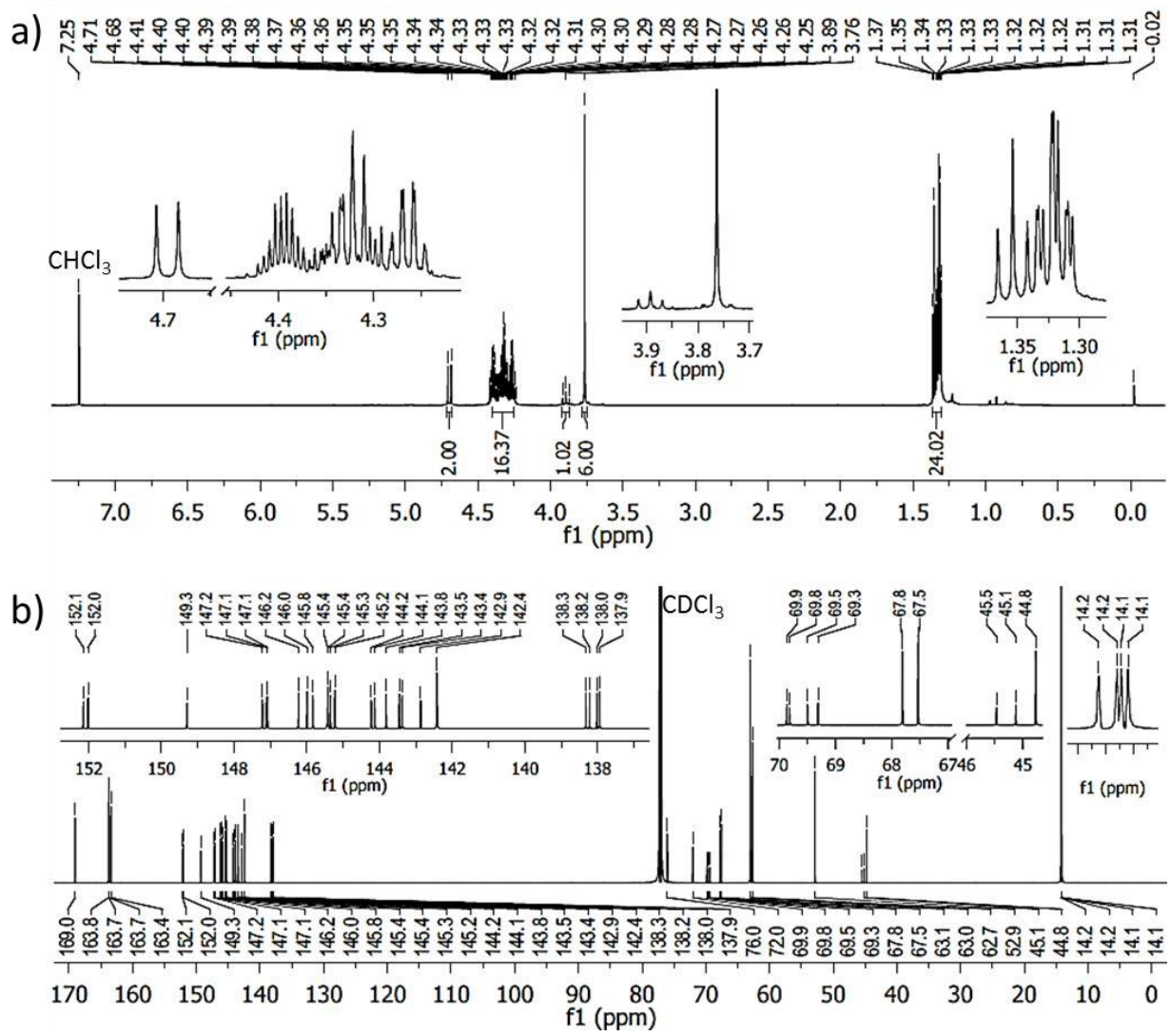

Figure S1. (a) ^{1}H- and (b) ^{13}C-NMR, 600 and 150 MHz, respectively; $CDCl_3$, 298 K for pentaadduct (ester).

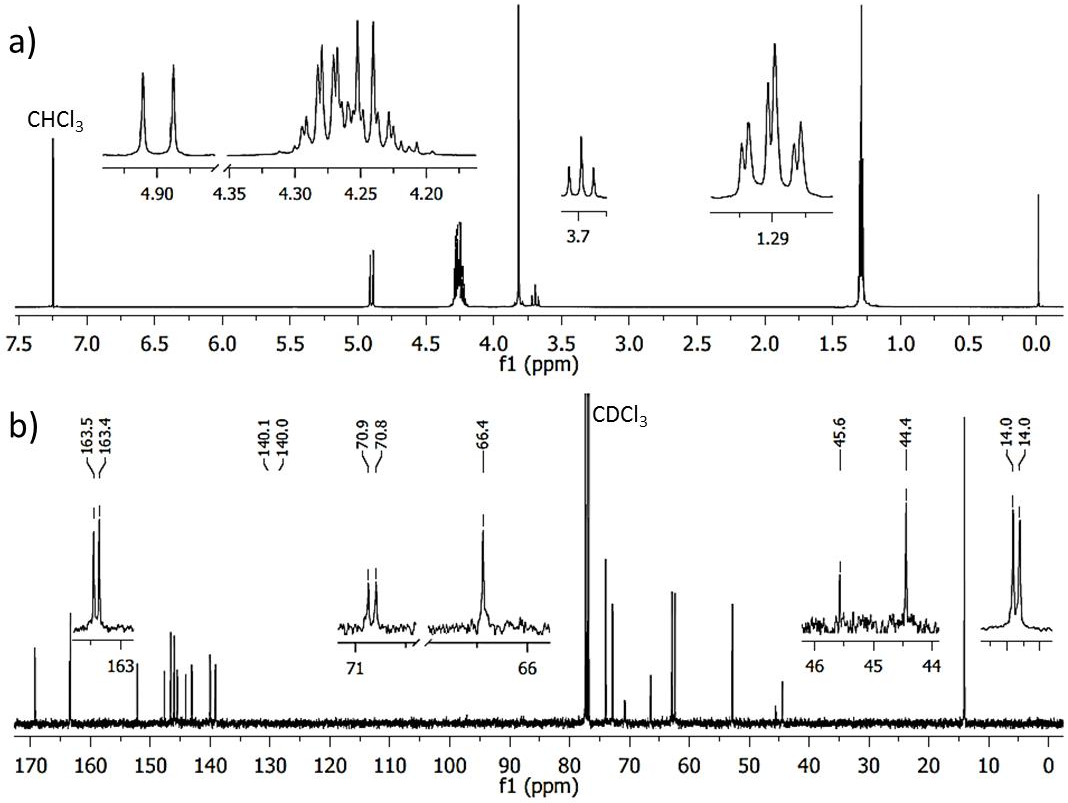

Figure S2. (a) ^{1}H- and (b) ^{13}NMR, 600 and 150 MHz, respectively; $CDCl_3$, 298 K for hexaadduct (ester).

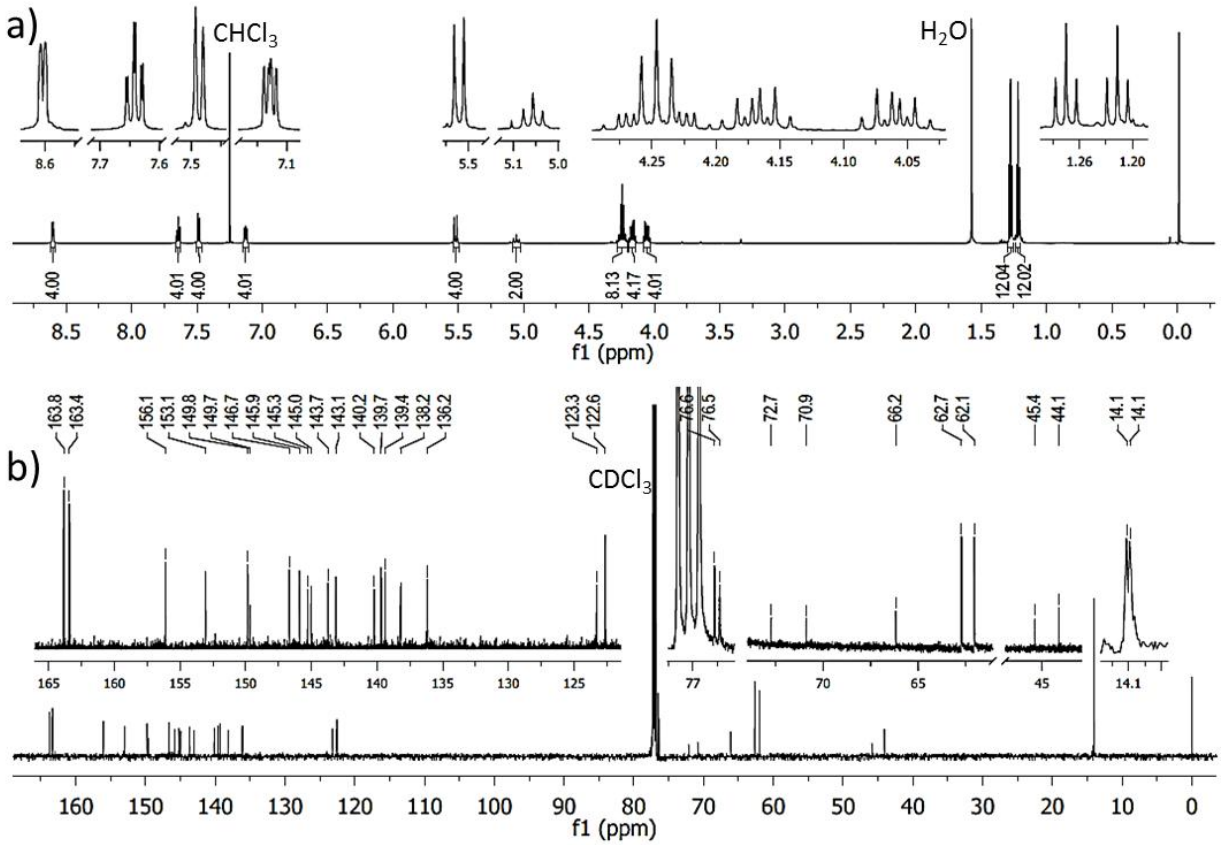

Figure S3. (a) ^{1}H- and b) ^{13}NMR, 600 and 150 MHz, respectively; $CDCl_3$, 298 K for hex adduct (pyridine).

Supporting information 2: The crystal structures for the penta and hexa adduct derivatives

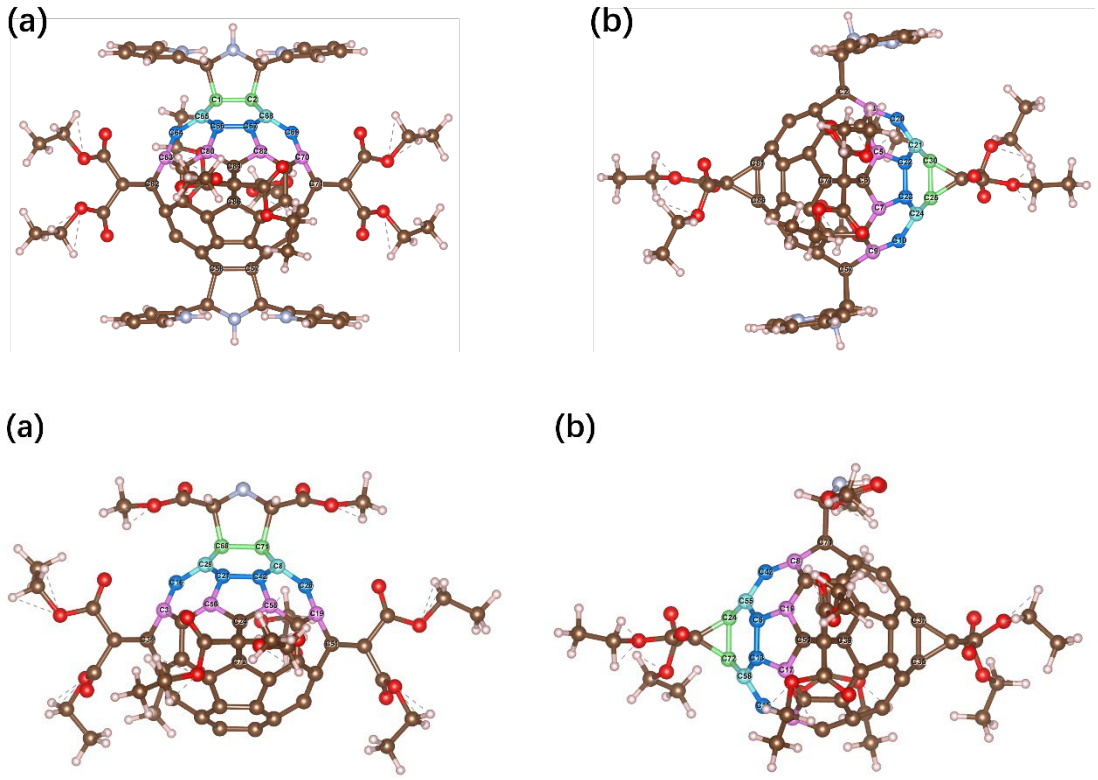

Figure S4. The crystal structures for the penta and hexa adducts derivatives.

Supporting Information 3: Electrochemical characterization of the electrode materials

Electrochemical measurements were performed in a three-electrode system at an electrochemical work-station (CHI 660D). 5 µL of each catalyst in toluene solution (containing 0.05 mg/ mL of catalyst) was deposited onto a 3 mm diameter glassy carbon electrode to reach a loading of approximately 3.57 µg·cm ^{2}. LSVs with, a scan rate of 2 mV·s^{-1}, were performed in 0.5 M H_2SO_4 (purged with pure Ar) using Ag/ AgCI (in 3M KC] solution) electrode as the reference electrode, a graphite rod as the counter electrode, and the glassy carbon electrode as the working electrode. All the LSV measurements were repeated at least 3 times to ensure reproducibility. All the potential was calibrated to a reversible hydrogen electrode (RHE).

Supporting information 4: Comparison table and Chronoamperometry Measurement.

Table 1. Efficiency compared to most recently reported Metal-Free catalysts

Materials	**Tafel slope (mV dec^{-1})**	**Onset potential (V) (E_{onset})**	**Overpotential @10 mA cm^{-2}/V**	**Electrolyte**	**References**
C_{60}	202.7	0.31	--	KOH (0.1 M)	[3]
C_{60}-$SWCNT_{15}$	120.8	0.11	0.380	KOH (0.1 M)	[3]
BINOL-CTF-10-500	41.04	0.066	0.311	H_2SO_4 (0.5 M)	[4]
10% F/BCN	82.0	-0.042	0.222	H_2SO_4 (0.5 M)	[5]
$NOPHC_{10}$-900	102	-0.18	0.290	KOH (1.0 M)	[6]
3h-N-GNS	115	-0.403	0.707	KOH (0.1 M)	[7]
BCN-1	100	-0.284	0.298	H_2SO_4 (0.5 M)	[8]
PCTF-10500	342	-0.114	0.227	H_2SO_4 (0.5 M)	[9]
G-12NP	67.3	--	0.106	H_2SO_4 (0.5 M)	[10]
P-rGO	46	--	0.440	H_2SO_4 (1.0 M)	[11]
NS-doped hierarchical np-graphene 500 °C	72	-0.12	-0.230	H_2SO_4 (0.5 M)	[12]
TpPAM	106	--	0.250	H_2SO_4 (0.5 M)	[13]
g-C_3N_4 nanoribbon-G	54	-0.080	0.207	H_2SO_4 (0.5 M)	[14]
S-CN/PC	84	-0.055	0.186	H_2SO_4 (0.5 M)	[15]
Penta adduct C_{60}	48	-0.045	0.075	H_2SO_4 (0.5 M)	This work

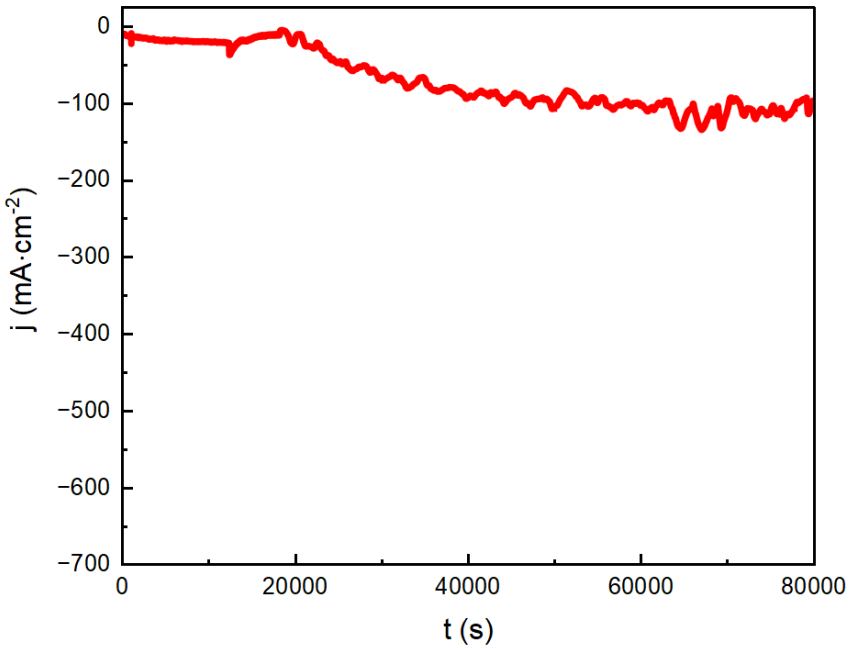

Figure S5. I-t measurements of the P-C_{60} for 80000 s at -0.10 V vs. RHE.

Supporting information 5: X-ray Photoelectron Spectroscopy (XPS) and Faradic efficiency

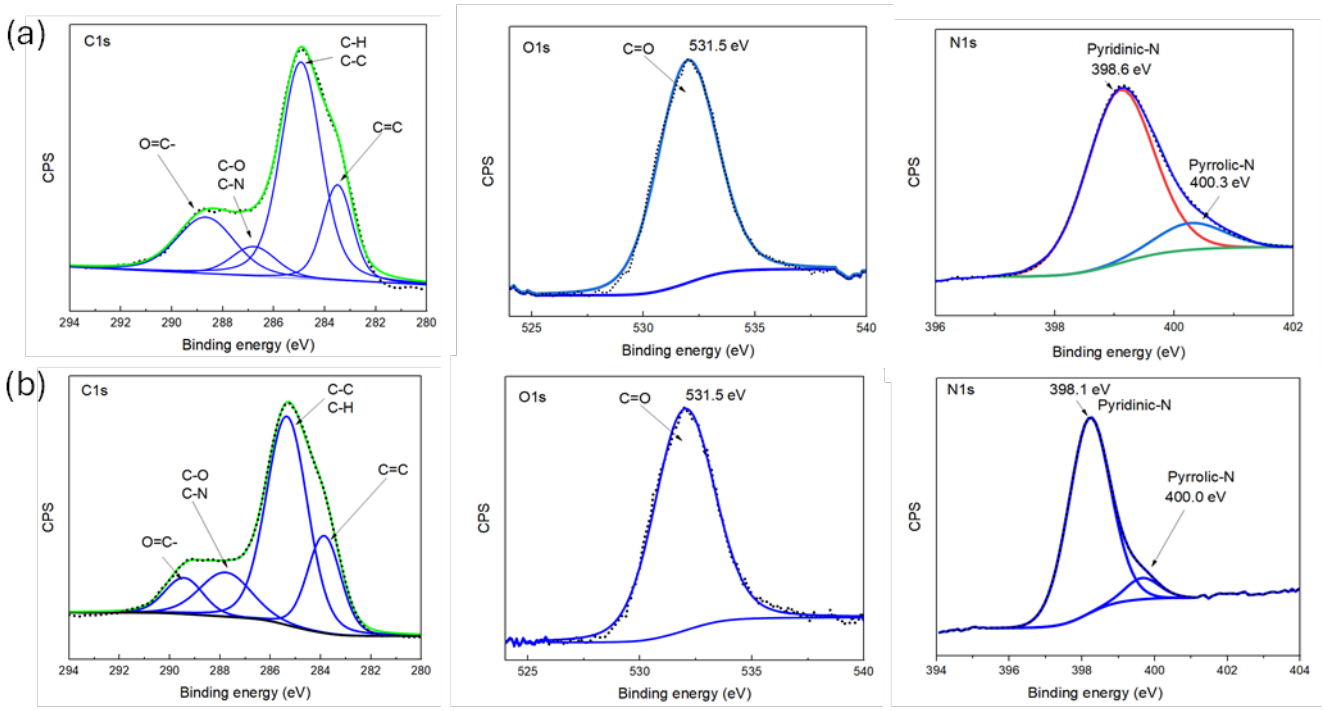

Figure S6. Represents the high-resolution XPS profile of P-C_{60} (a) before and (b) after a chrono-amperometric experiment ($E_{applied}$=-0.10 V vs RHE).

The chemical state of carbon, oxygen, and nitrogen was determined by analyzing the high-resolution spectra of the C1s, O1s, and N1s before and after electrocatalysis (Figure S6). The presence of several different chemical states was related to the specific chemical bonding with the surrounding elements of

the Penta adduct. The analysis of the main component indicated that carbon existed in several different chemical states (see deconvoluted C1s line in Figure S6a). The chemical state with the lowest binding energy of 283.42 eV was related to the occurrence of silicone contamination. The most pronounced peak in the spectra of both samples was located at 284.82 eV and was related to the presence of C–H or C–C bonds. Interestingly, oxygen and nitrogen-containing groups C–O or C–N (at 287.6 eV) were detected, whereas the presence of the typical carbonyl group (C=O) (288.5 eV) was also detected. The O1s line indicated a carbon-oxygen bond; slightly below 532 eV. The deconvoluted N1s line indicated the presence of four components; the most pronounced component at 398.6 eV was related to basic nitrogen (pyridinic type), and the chemical state at 401.3 eV was related to pyrrolic N.

Faradic efficiency experiments

Controlled-potential electrolysis measurements were conducted in a sealed, two-chambered H-cell, where the first chamber contained the working and reference electrodes in 50 mL of 0.5 M H_2SO_4(aq) with 0.2 mM P-C60. The second chamber held the auxiliary electrode in 25 mL of 0.5 M H_2SO_4. The chambers were separated by a fine-porosity glass frit. Glassy carbon electrode served as the working and auxiliary electrodes, submerged to expose approximately 64 cm^2 of the plate to the electrolyte solution. An Ag/AgCl electrode, separated from the solution by a Vycor frit, functioned as the reference electrode. Prior to each electrolysis experiment, the cell was purged with N_2 for 30 minutes and sealed under an N^2 atmosphere. In 24-hour experiments, the volume of H_2 evolved was quantified from the headspace of the first chamber. Faradaic efficiencies were determined by dividing the measured H_2 produced by the expected amount based on the charge passed during controlled-potential electrolysis measurements. For longer 24-hour experiments, H_2 evolution was quantified by measuring the volumetric displacement of headspace gas **(see Table S2, Supporting Information 5)**.

Reaction at cathode
Charge on 1e = 1F
1F = 96500 C
F or balanced equation
96500 C deposits 2 g H_2
1C deposits 2/96500 g H_2
Q = i*t where i is the current and t is the time of the experiment.
n (e) = Q / 96500
$2H+ + 2e = H_2$
(mole) = n(e)* 1 mole H_2 /2

Table S2. The charge passed, Measured hydrogen volume, and Faradaic Efficiencies at different times for one day HER electrolysis measurements.

time	Q (C)	V (ml)	FE (%)
24	**1104**	**11.5**	**89 %**

Supporting information 6: DFT

The Density functional theory (DFT) as implemented in the Vienna Ab-initio Simulation Package (VASP) code was employed to perform the calculations.[16, 17]The generalized gradient approximation[18] in the form of the Perdew−Burke−Ernzerhof functional[19] was used to described exchange-correlation interactions.

The Blöchl's all-electron, frozen-core projector augmented wave (PAW) method[20] were used to represent nuclei and core electrons. The van der Waals interaction was described by using the empirical correction in Grimme's scheme, i.e., DFT+D3[21] for all the calculations. The electron wave functions were expanded using the plane waves with a cut off energy of 500 eV. The geometries were optimized until the energy and the force were converged to 0.001 eV/Å and 10^{-6} eV, respectively. A Gamma point in reciprocal space was used for the k-point sampling during geometry optimization.

The free energy of the adsorption atomic hydrogen (ΔG_{H^*}) is calculated as following:

$$\Delta G_{H^*} = \Delta E_H - \Delta E_{ZPE} - T\Delta S_H \quad \text{(s1)}$$

ΔE_H represents the differential hydrogen adsorption energy and can be described as:

$$\Delta E_H = E_{H*} - E^* - \frac{1}{2}H_2 \quad \text{(s2)}$$

where * denotes the catalyst. E_{H*}, E^* and $\frac{1}{2}H_2$ represents total energies of catalyst plus one H adsorbed hydrogen atoms, the total energies of catalyst without adsorbed hydrogen atoms and H_2 gas, respectively. ΔE_{ZPE} is the difference corresponding to the zero-point energy between the adsorbed state and the gas phase. The contributions from the catalysts to both ΔEZPE and ΔSH are small and can be neglected. Therefore, ΔEZPE is obtained by:[22]

$$\Delta E_{ZPE} = E_{ZPE}^H - \frac{1}{2}E_{ZPE}^{H_2} \quad \text{(s3)}$$

where the E_{ZPE}^H is the zero-point energy of one adsorbed atomic hydrogen on the catalyst surface without the contribution of the catalyst. $E_{ZPE}^{H_2}$ is the zero-point energy of H_2 in the gas phase.

The S_H is the entropy of H_2 gas at the standard condition. The ΔS_H can be obtained by:

$$\Delta S_H \cong \frac{1}{2}S_{H_2}^0 \quad \text{(s4)}$$

Therefore, the overall corrections can be obtained as:[9]

$$\Delta E_H = E_{H^*} - \frac{1}{2}E_{H_2} - E^* \quad \text{(s5)}$$

where * refers to the catalyst used for hydrogen evolution. E_{H^*}, E_{H2}, and E* represent the total energies of catalyst plus one adsorbed hydrogen atom, gas H_2, and catalyst, respectively. Thus, the Gibbs free energy change can be written as:

$$\Delta G_{H^*} = \Delta E_H + 0.16\ eV \quad \text{(s6)}$$

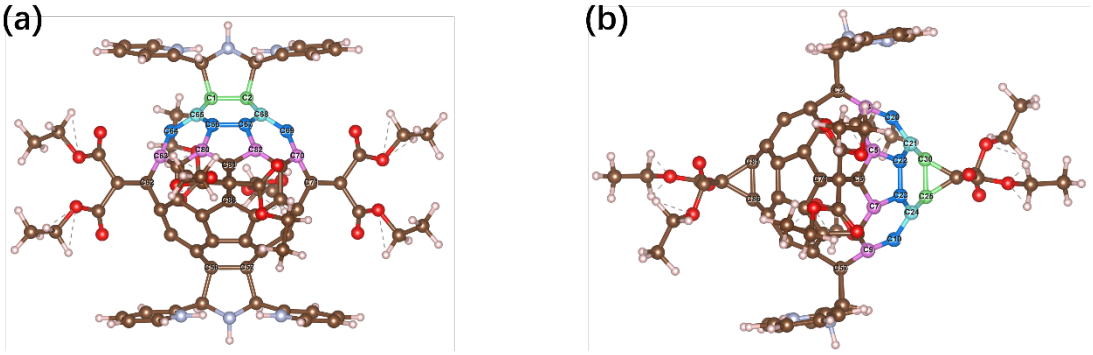

Figure S7. The different types of C atoms according to the distance between the C atoms of C_{60} and the ligands for Hexa-C_{60}, the cyan, blue and pink atoms represent the first, second and third nearest C atoms, respectively.

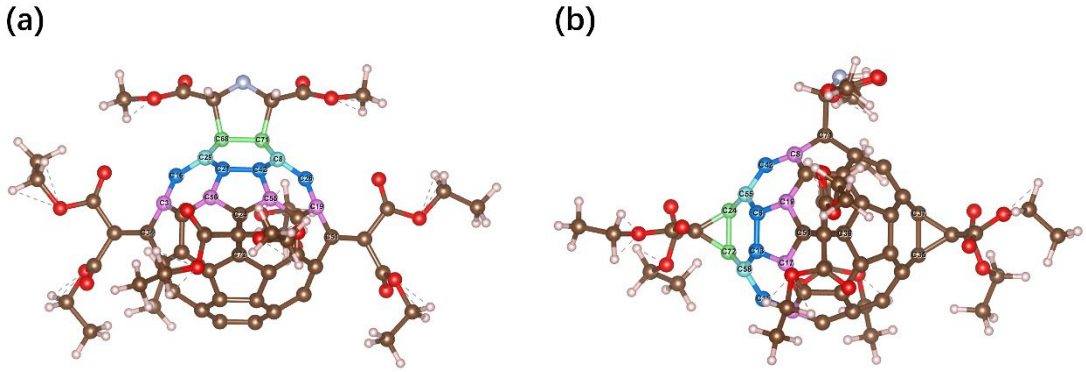

Figure S8. The different types of C atoms according to the distance between the C atoms of C_{60} and the ligands for Penta-C_{60}, the cyan, blue and pink atoms represent the first, second and third nearest C atoms, respectively.

References:

(1) Schwenninger, R.; Müller, T.; Kräutler, B. Concise Route to Symmetric Multiadducts of [60]Fullerene: Preparation of an Equatorial Tetraadduct by Orthogonal Transposition. *Journal of the American Chemical Society* **1997**, *119* (39), 9317-9318. DOI: 10.1021/ja971875p.
(2) Castro, E.; Azmani, K.; Garcia, A. H.; Aghabali, A.; Liu, S.; Metta-Magana, A. J.; Olmstead, M. M.; Rodríguez-Fortea, A.; Poblet, J. M.; Echegoyen, L. Cover Feature: Unusual C2h-Symmetric trans-1-(Bis-pyrrolidine)-tetra-malonate Hexa-Adducts of C60: The Unexpected Regio- and Stereocontrol Mediated by Malonate–Pyrrolidine Interaction (Chem. Eur. J. 63/2017). *Chemistry – A European Journal* **2017**, *23* (63), 15841-15841. DOI: https://doi.org/10.1002/chem.201703999.
(3) Gao, R.; Dai, Q.; Du, F.; Yan, D.; Dai, L. C_{60}-adsorbed single-walled carbon nanotubes as metal-free, pH-universal, and multifunctional catalysts for oxygen reduction, oxygen evolution, and hydrogen evolution. *Journal of the American Chemical Society* **2019**, *141* (29), 11658-11666.
(4) Jena, H. S.; Krishnaraj, C.; Parwaiz, S.; Lecoeuvre, F.; Schmidt, J.; Pradhan, D.; Van der Voort, P. Illustrating the role of quaternary-N of BINOL covalent triazine-based frameworks in oxygen reduction and hydrogen evolution reactions. *ACS Applied Materials Interfaces* **2020**, *12* (40), 44689-44699.
(5) Ahsan, M. A.; He, T.; Eid, K.; Abdullah, A. M.; Curry, M. L.; Du, A.; Puente Santiago, A. R.; Echegoyen, L.; Noveron, J. C. Tuning the intermolecular electron transfer of low-dimensional and metal-free BCN/C_{60} electrocatalysts via interfacial defects for efficient hydrogen and oxygen electrochemistry. *Journal of the American Chemical Society* **2021**, *143* (2), 1203-1215.
(6) Huang, S.; Meng, Y.; Cao, Y.; He, S.; Li, X.; Tong, S.; Wu, M. N-, O-and P-doped hollow carbons: metal-free bifunctional electrocatalysts for hydrogen evolution and oxygen reduction reactions. *Applied Catalysis B: Environmental* **2019**, *248*, 239-248.
(7) Swaminathan, J.; Enayat, S.; Meiyazhagan, A.; Robles Hernandez, F. C.; Zhang, X.; Vajtai, R.; Vargas, F. M.; Ajayan, P. M. Asphaltene-derived metal-free carbons for electrocatalytic hydrogen evolution. *ACS applied materials interfaces* **2019**, *11* (31), 27697-27705.
(8) Chhetri, M.; Maitra, S.; Chakraborty, H.; Waghmare, U. V.; Rao, C. Superior performance of borocarbonitrides, $B_xC_yN_z$, as stable, low-cost metal-free electrocatalysts for the hydrogen evolution reaction. *Energy Environmental Science* **2016**, *9* (1), 95-101.
(9) Jena, H. S.; Krishnaraj, C.; Satpathy, B. K.; Rawat, K. S.; Leus, K.; Veerapandian, S.; Morent, R.; De Geyter, N.; Van Speybroeck, V.; Pradhan, D. Phosphorus Covalent Triazine Framework-Based Nanomaterials for Electrocatalytic Hydrogen Evolution Reaction. *ACS Applied Nano Materials* **2023**, *6* (24), 22684-22692.
(10) Wu, H.; Chen, Z.; Wang, Y.; Cao, E.; Xiao, F.; Chen, S.; Du, S.; Wu, Y.; Ren, Z. Regulating the allocation of N and P in codoped graphene via supramolecular control to remarkably boost hydrogen evolution. *Energy Environmental Science* **2019**, *12* (9), 2697-2705.

(11) Khalid, M.; Varela, H. A general potentiodynamic approach for red phosphorus and sulfur nanodot incorporation on reduced graphene oxide sheets: metal-free and binder-free electrodes for supercapacitor and hydrogen evolution activities. *Journal of Materials Chemistry A* **2018**, *6* (7), 3141-3150.
(12) Chen, L.; Han, J.; Ito, Y.; Fujita, T.; Huang, G.; Hu, K.; Hirata, A.; Watanabe, K.; Chen, M. Heavily doped and highly conductive hierarchical nanoporous graphene for electrochemical hydrogen production. *Angewandte Chemie International Edition* **2018**, *57* (40), 13302-13307.
(13) Patra, B. C.; Khilari, S.; Manna, R. N.; Mondal, S.; Pradhan, D.; Pradhan, A.; Bhaumik, A. A metal-free covalent organic polymer for electrocatalytic hydrogen evolution. *ACS Catalysis* **2017**, *7* (9), 6120-6127.
(14) Zhao, Y.; Zhao, F.; Wang, X.; Xu, C.; Zhang, Z.; Shi, G.; Qu, L. Graphitic carbon nitride nanoribbons: graphene-assisted formation and synergic function for highly efficient hydrogen evolution. *Angewandte Chemie International Edition* **2014**, *53* (50), 13934-13939.
(15) Pei, Z.; Gu, J.; Wang, Y.; Tang, Z.; Liu, Z.; Huang, Y.; Huang, Y.; Zhao, J.; Chen, Z.; Zhi, C. Component matters: Paving the roadmap toward enhanced electrocatalytic performance of graphitic C_3N_4-based catalysts via atomic tuning. *ACS nano* **2017**, *11* (6), 6004-6014.
(16) Kresse, G.; Furthmüller, J. Efficiency of ab-initio total energy calculations for metals and semiconductors using a plane-wave basis set. *Computational materials science* **1996**, *6* (1), 15-50.
(17) Kresse, G.; Furthmüller, J. Efficient iterative schemes for ab initio total-energy calculations using a plane-wave basis set. *Physical review B* **1996**, *54* (16), 11169.
(18) Perdew, J. P.; Burke, K.; Ernzerhof, M. Generalized gradient approximation made simple. *Physical review letters* **1996**, *77* (18), 3865.
(19) Perdew, J. P.; Ernzerhof, M.; Burke, K. Rationale for mixing exact exchange with density functional approximations. *The Journal of chemical physics* **1996**, *105* (22), 9982-9985.
(20) Blöchl, P. E. Projector augmented-wave method. *Physical review B* **1994**, *50* (24), 17953.
(21) Grimme, S. Semiempirical GGA-type density functional constructed with a long-range dispersion correction. *Journal of computational chemistry* **2006**, *27* (15), 1787-1799.
(22) Tsai, C.; Abild-Pedersen, F.; Nørskov, J. K. Tuning the MoS2 edge-site activity for hydrogen evolution via support interactions. *Nano letters* **2014**, *14* (3), 1381-1387.